Regional gravity field recovery from GRACE using position optimized radial base functions

M. Weigelt, M. Antoni, W. Keller
Institute of Geodesy, Universität of Stuttgart, Geschwister-Scholl-Str. 24D, 70174 Stuttgart, Germany

Abstract. Global gravity solutions are generally influenced by degenerating effects such as insufficient spatial sampling and background models among others. Local irregularities in data supply can only be overcome by splitting the solution in a global reference and a local residual part. This research aims at the creation of a framework for the derivation of a local and regional gravity field solution utilizing the so-called line-of-sight gradiometry in a GRACE-scenario connected to a set of rapidly decaying base functions. In the usual approach, the latter are centered on a regular grid and only the scale parameter is estimated. The resulting poor condition of the normal matrix is counteracted by regularization. By contrast, here the positions as well as the shape of the base functions are additionally subject to the estimation process. As a consequence, the number of base functions can be minimized. The analysis of the residual observations by local base functions enables the resolution of details in the gravity field which are not contained in the global spherical harmonic solution. The methodology is tested using simulated as well as real GRACE data.

Keywords. GRACE, line-of-sight gradiometry, radial base functions, non-linear optimization

1 Introduction

Local gravity field recovery has the advantage that the solutions can be tailored to the region of interest and can make better use of the available data. For example, global ocean tide models currently do not take into account the ice coverage in the winter months in some areas, e.g. in the Hudson Bay (Canada). Local and regional ocean tide models are available but cannot be applied due to the missing global support. Another example is the groundtrack pattern which defines the spatial sampling and the resolution of the gravity field model. A global solution is primarily governed by the data distribution at the equator which is sparser than in high-latitude areas, since the orbit converges towards the poles. As a consequence spurious signal is introduced and aliasing occurs. Maybe the most convincing motivation for regional analysis can be seen in figure 1. The top panel shows the comparison of the K-Band derived range rate vs. the relative velocity of the two GRACE satellites projected on the line of sight for an arc crossing the Himalayan mountains in August 2003. The relative velocities have been calculated by integrating a 6-min arc for each satellite using GGM02S until degree and order 110, which is the suggested maximum degree of this global GRACE-only model (*Tapley et al.*, 2005). The bottom panel shows the profile of the topography along the groundtrack of the barycenter, defined as the arithmetic mean of the positions of the satellites. As the satellites cross the Himalayan mountain ridge, residual signal of $\delta\dot{\rho} \approx 2\,\mu\mathrm{m/s}$ is visible. Repeating the same procedure using GGM02C until degree and order 150, which incorporates also altimetric and terrestrial data, the topographic correlation is reduced. Consequently, a global spherical harmonic analysis using satellite data only makes not fully use of the available information and an improvement might be possible using local methods.

The idea of regional gravity field modeling from GRACE-data is not new. For example, *Eicker* (2008) adopts radial base functions on a spherical grid to refine the gravity solutions. The in-situ measurements are derived by the short-arc method

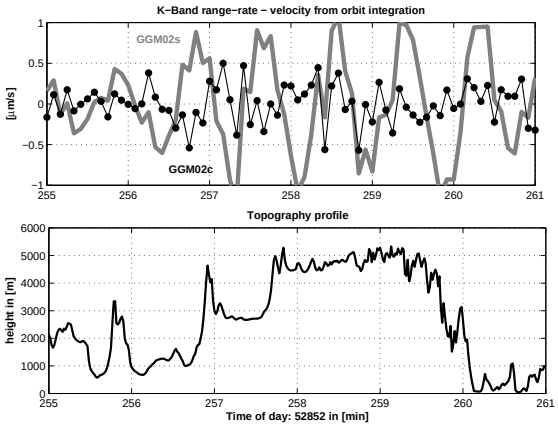

Figure 1. K-band observation vs. velocity differences (top); profile of the topography for an arc crossing the Himalayan mountains in August 2003 (bottom)

developed by *Mayer-Gürr* (2006). *Han and Simons* (2008) utilize the energy balance approach and Slepian functions to detect the gravity change caused by the Sumatra-Andaman earthquake. *Schmidt et al.* (2007) applies multi-resolution analysis and spherical wavelets to the CHAMP and GRACE missions. All show that a regional refinement leads to improved solutions in the area of interest.

This paper will introduce an alternative approach for the estimation of local gravity field recovery which consists of two steps. First, in-situ observables will be derived by the line-of-sight (LOS) gradiometry (*Keller and Sharifi*, 2005). Second, the local recovery will also make use of radial base functions as in *Eicker* (2008) but beside the scale parameter also their position and their shape parameter are subject to an optimization process. The number of base functions is found in an iterative procedure which will avoid instabilities due to overparametrization and does not need regularization. However, the relation of the in-situ observable to the radial base functions requires to solve a non-linear least-squares problem resulting in a high computational effort.

The paper will start with the derivation of the basic equation for the calculation of the in-situ measurements in section 2.1 followed by the introduction of the radial base functions in section 2.2 and the optimization procedure in section 2.3. Possible error sources are discussed in section 2.4 before results using simulated and real GRACE-data are presented in section 3 proving the applicability of approach.

2 Data processing

The primary observables of the GRACE system are the K-band derived range rate and range acceleration between the two satellites. The basic geometry of the GRACE system has already been depicted in *Rummel et al.* (1978) and is shown in figure 2. The aim is to connect the measurements via the line-of-sight gradiometry to the radial base functions.

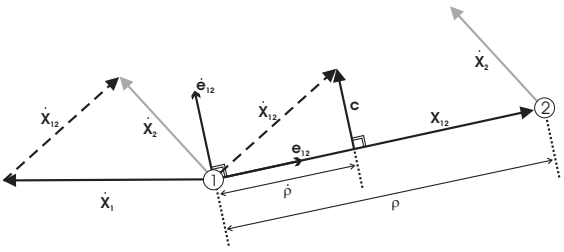

Figure 2. Geometric setup of the GRACE-system (*Rummel et al.*, 1978)

2.1 Line-of-sight gradiometry

The line-of-sight gradiometry relates the observables to the gravity tensor projected on the line of sight, which creates a direct link to the gravity field geometry, i.e. the curvature of the field in the evaluation point. At the cost of a slightly increased noise level due to differentiation, it yields an in-situ observation that is less affected by the orbital history and can be connected to the barycenter of the satellites. The range rate $\dot{\rho}$ is related to the relative velocity $\dot{\mathbf{X}}_{12}$ by projection on the line of sight which is expressed by the unit vector pointing from satellite 1 to 2:

$$\dot{\rho} = \dot{\mathbf{X}}_{12} \cdot \mathbf{e}_{12}. \tag{1}$$

Taking the derivative yields:

$$\ddot{\rho} = \ddot{\mathbf{X}}_{\mathbf{12}} \cdot \mathbf{e}_{12} + \dot{\mathbf{X}}_{12} \cdot \dot{\mathbf{e}}_{12}. \tag{2}$$

The first term on the right hand side can be connected to the gradient of the potential at the position of each satellite. Reformulating the change of the line-of-sight vector $\dot{\mathbf{e}}_{12}$ as a combination of the relative velocity vector and the range rate (*Rummel et al.*, 1978) and rearranging the equation yields an expression which is generally referred to as the *differential gravimetry approach*:

$$(\nabla V_2 - \nabla V_1) \cdot \mathbf{e}_{12} = \ddot{\rho} + \frac{\dot{\rho}^2}{\rho} - \frac{\|\dot{\mathbf{X}}_{12}\|}{\rho}. \tag{3}$$

Dividing both sides by the range ρ, the left hand side contains the discretized first order differential of the gravity gradient and thus can be approximated by the projected gravity tensor $\mathbf{G}$:

$$\mathbf{e}_{12}^T \mathbf{G} \mathbf{e}_{12} + \mathscr{O}^2 = \frac{\ddot{\rho}}{\rho} + \frac{\dot{\rho}^2}{\rho^2} - \frac{\|\dot{\mathbf{X}}_{12}\|}{\rho^2}. \tag{4}$$

The left hand side contains the first order and the abbreviation for higher order terms $\mathscr{O}^2$. *Keller and Sharifi* (2005) demonstrated that the higher order terms cannot be neglected but the consideration of the linear term is sufficient if an adequate *a priori* field is subtracted and the observable is reduced to a residual quantity:

$$\mathbf{e}_{12}^T \mathbf{G} \mathbf{e}_{12} = \frac{\ddot{\rho}}{\rho} + \frac{\dot{\rho}^2}{\rho^2} - \frac{\|\dot{\mathbf{X}}_{12}\|}{\rho^2} - \frac{1}{\rho}\left(\nabla V_2^0 - \nabla V_1^0\right) \cdot \mathbf{e}_{12}. \tag{5}$$

Working on the residual signal is not a disadvantage for regional applications, since long-wavelength features have to be reduced anyway. The final step is to include all gravitational and non-gravitational disturbing forces $\mathbf{g}^i$ which need to be calculated or measured for each satellite separately. Their difference is

also projected on the line of sight:

$$\mathbf{e}_{12}^T \mathbf{G} \mathbf{e}_{12} = \frac{\ddot{\rho}}{\rho} + \frac{\dot{\rho}^2}{\rho^2} - \frac{\|\dot{\mathbf{X}}_{12}\|}{\rho^2} - \frac{1}{\rho} \sum_i \mathbf{g}_{12}^i \cdot \mathbf{e}_{12} - \frac{1}{\rho} \left(\nabla V_2^0 - \nabla V_1^0 \right) \cdot \mathbf{e}_{12}. \tag{6}$$

The equation contains quantities taken from the K-band ranging system as well as from GPS, namely the relative velocity of the two satellites. The poorer accuracy of the latter theoretically prevents the implementation but *Keller and Sharifi* (2005) showed also that practically they can be replaced by velocities derived using numerical integrated orbits derived from a known *a priori* gravity field. By equation (6) in-situ observations along the orbit can be calculated and can be connect to a function with local support, i.e. the radial base functions.

2.2 Radial Base Functions

The starting point is the description of the potential in terms of radial base functions Ψ_b:

$$V(\lambda, \vartheta, r) = \frac{GM}{R} \sum_{b=1}^{B} \eta_b \Psi_b(\lambda, \vartheta, r), \tag{7}$$

where η_b is the scale parameter. The aim of our approach is to keep B, i.e. the maximum number of base functions, as low as possible in order to avoid overparametrization. Every base function Ψ_b is given as:

$$\Psi_b(\lambda, \vartheta, r) = \sum_{n=0}^{N} \left(\frac{R}{r} \right)^{n+1} \sigma_b(n) P_n(\cos \varpi_b) \tag{8}$$

and has its individual and degree dependent shape parameter $\sigma_b(n)$. N denotes the maximum degree of development and ϖ_b is the spherical distance between the computational position (λ, ϑ) and the center of the base function (λ_b, ϑ_b). In order to connect the base functions to the line-of-sight gradiometry, the second derivative in the flight direction y has to be taken. According to *Koop* (1993):

$$\frac{\partial^2 V}{\partial y^2} = \frac{1}{a^2} \frac{\partial^2 V}{\partial u^2} + \frac{1}{a} \frac{\partial V}{\partial r}, \tag{9}$$

i.e. the derivative in the flight direction can be replaced by the second derivative towards the argument of latitude u and the first radial derivative in combination with the osculating (instantaneous) semi-major axis. Since in equation (7) only Ψ_b is dependent on r and u, it is sufficient to take the derivative of the base function itself:

$$\frac{\partial^2 \Psi_b}{\partial y^2} = \frac{1}{a^2} \sum_{n=0}^{N} \sigma_b(n) \left(\frac{R}{r} \right)^{n+1} \left\{ \left(\frac{\partial \zeta_b}{\partial u} \right)^2 P_n''(\zeta_b) + \left(2 \frac{-(n+1) e \sin E}{\sqrt{1-e^2}} \frac{\partial \zeta_b}{\partial u} - \zeta_b \right) P_n'(\zeta_b) + \left(\frac{(n+1) e^2 \sin^2 E}{1-e^2} - \frac{re \cos E}{a(1-e^2)} - \frac{a}{r} \right) (n+1) P_n(\zeta_b) \right\} \tag{10}$$

where the abbreviation $\zeta_b := \cos \varpi_b$ is introduced. $P_n'(\zeta_b)$ and $P_n''(\zeta_b)$ denote the first and second derivatives of the Legendre-polynomials, E the eccentric anomaly and e the eccentricity of the orbit.

The final step is to connect the second derivative of the radial base function in flight direction to the linear term of the line-of-sight gradiometry. Thus, the model is applied to the residual field and model inconsistencies need to be considered.

$$\mathbf{e}_{12}^T \mathbf{G} \mathbf{e}_{12} = \frac{GM}{R} \sum_{b=1}^{B} \eta_b \frac{\partial^2 \Psi_b}{\partial y^2} + \varepsilon \tag{11}$$

Equation (11) forms the basic observation equation for the subsequent optimization process.

2.3 Optimization of the parameters

Commonly, the central position (λ_b, ϑ_b) of each base function is fixed on a regular grid and the shape parameter $\sigma_b(n)$ is derived from Kaula's rule (*Kaula*, 1966):

$$\sigma_b^2(n) = (2n+1) \frac{10^{-10}}{n^4} \tag{12}$$

Only the scale factors η_b are subject to an estimation process. The problem remains linear but numerous base functions might be necessary to achieve reasonable accuracies. It leads quickly to an overparametrization which needs to be counteracted by regularization (*Eicker*, 2008).

An alternative approach is to estimate all parameters of the radial base functions $(\lambda_b, \vartheta_b, \eta_b, \sigma_b(n))$ from the data directly. Thus, overparametrization is avoided by just using a minimal number of bases. Reviewing equation (10), it is evident that the optimization of the position and the shape parameter results in a non-linear least-squares adjustment, which needs to be solved iteratively.

Figure 3 shows the workflow of the iterative optimization process. Beginning with the preprocessed pseudo-observables of the line-of-sight gradiometry, a residual quantity is formed by subtracting the long wavelength part of the gravity field, cf. equation (6).

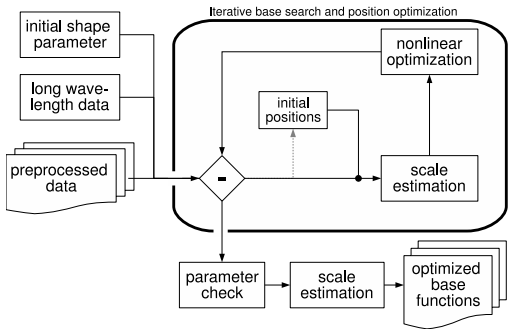

Figure 3. Workflow of the algorithm

The area of calculation has been chosen to be bigger than the area of interest in order to deal with edge effects later on. Empirically, we found that adding a frame of 3° is sufficient. The shape parameters are modeled by the exponential relationship

$$\sigma_b(n) = \sigma_b^n. \tag{13}$$

The localizing properties and the convergence of the base function is ensured if the σ is within the interval $[0.9, 1]$. Since we found in numerous test that most shape parameters converge to 1, we chose $\sigma = 0.97$ as the starting value in order to keep the number of iterations small.

Entering the iterative base search, initial values for the central positions of the base functions and the scale parameters η_b have to be estimated first. A reasonable choice for the positions are the minima and maxima of the residual field. By interpolating a copy of the data onto a 0.5° grid and smoothing it with a binomial filter, it is ensured that outliers are removed and the initial positions are not too close together. The scale parameters are estimated using a standard least-squares adjustment since they are linearly related according to equation (7).

These initial values are improved by a nonlinear least-squares solver, which is based on the Levenberg-Marquardt algorithm (*Marquardt*, 1963). Boundary restrictions ensure that the central positions do not change by more than 5° and the shape parameters remain in the aforementioned interval $[0.9, 1]$. The scale parameters η_b are not restricted. In case of convergence, a synthesis of the estimated base functions is calculated and subtracted from the input field in order to get a new residual field.

$$\delta V_{i+1} = \delta V_i - \frac{GM}{R} \sum_{b=1}^{B_i} \eta_b \frac{\partial^2 \Psi_b}{\partial y^2}. \tag{14}$$

The procedure is repeatedly applied to increase the number of base functions but terminated if the center of the base functions get too close together, the scale factors become unreasonably small or the standard deviations are larger than the estimated value itself.

In the final steps of the procedure, the estimated parameters are tested for inconsistencies, e.g. base functions are located outside the area of interest. If base functions need to be rejected, the scale factors are readjusted. Finally, edge effects are minimized by removing the 3° frame and the user is provided with optimized parameters for the base functions.

2.4 Error sources

In the local refinement, the residual signal consists of gravity signal, noise and spurious signal due to aliasing and modeling errors. Note that gravity is highly correlated with the topography whereas the correlation of all other components with the topography is generally minor.

1. Aliasing occurs due to an undersampling of a signal. If the temporal sampling along the orbit is not sufficient, signal or parts of it cannot be recovered from the data and will alias into other frequencies. The effect can be minimized by removing the signal using appropriate models. However, their accuracy is limited which is currently considered as one of the reason that GRACE does not match the expected baseline accuracy, e.g. *Kanzow et al.* (2005). Spatial aliasing takes place if the sampling in the spatial domain is insufficient. The solution becomes especially degraded if GRACE passes a repeat mode, e.g. *Wagner et al.* (2006).
2. Modeling errors are caused by an insufficient mathematical and/or stochastic representation of the signal. Considering our approach, the LOS gradiometry introduces a linearization error which can be minimized by the subtraction of an *a priori* field as already mentioned (*Keller and Sharifi*, 2005). Gravitational disturbing forces are considered but are limited by the accuracy of their underlying model, e.g. *Han et al.* (2004). Non-gravitational forces are measured by the accelerometers onboard but are biased and scaled due to instrument effects. Corrections have to be estimated from the data which in turn are also limited in their accuracy (*Perosanz et al.*, 2005).
3. Any estimation process can be affected by under- or overparametrization which is here avoided due to the iterative search. However, the Levenberg-Marquardt algorithm does not necessarily find the global minimum and might converge to a local one instead (*Ortega and Rheinboldt*, 1970). This effect can be minimized by using the best available initial values.

3 Results

Having outlined the algorithm, the applicability of the approach can be tested. In a first step, simulated data is used to test for modeling errors. Subsequently, the method is applied to GRACE. Note that our primary intention is here to validate the methodology and its applicability to real data. Results using real GRACE data are preliminary and need to be cross-checked by e.g. GPS leveling.

3.1 Simulation

For the closed-loop simulation, 12 base functions were hidden in the area of the Mediterranean sea. The input signal ranges from -483 mE to 257 mE with a RMS $= 207.4$ mE and is two orders of magnitude stronger than the residual signal in the case of real data, which is desired here in order to reveal modeling errors. The left panel of figure 4 shows the difference between input and estimated signal, hereafter called approximation. Obviously, some type of 'trackiness' remains which is likely related to the geometry of the system. Since the pseudo-observables represent the second derivative along the line of sight, leakage will primarily occur in the direction of travel which is practically in the north-south direction. For the quantification of the fit, we use the ratio of the standard deviation between the observed and the approximation in percent:

$$Q = \frac{\mathrm{STD}(\text{approximation})}{\mathrm{STD}(\text{signal})} \cdot 100, \qquad (15)$$

The field is recovered with a Q of 98% and a RMS of 37.9 mE. Since a full recovery is unlikely without the usage of numerous base functions, the fit can be considered as an excellent result. Interestingly, the algorithm used 12 base functions but the location of the estimated base functions (●) differs significantly from the original positions (♦), cf. the right panel of figure 4. Nevertheless, the input signal is represented almost as good by the new set of base functions as by the original one. This is a nice depiction of the inverse problem of geodesy and visualizes that a local minimum has been found in the adjustment.

3.2 Real GRACE data

Generally, the residual signal of real GRACE data is noisy and contains, besides signal from the aforementioned error sources, a weak gravity component. In this test we are aiming at the recovery of the latter for an area in the Himalaya using level 1B GRACE data, which is provided by the Physical Oceanography Distributed Active Archive Center at the NASA Jet Propulsion Laboratory. The corresponding global gravity field solution for each month is provided by the GeoForschungsZentrum Potsdam (Rel. 4) (*Schmidt et al.*, 2006).

Our first method of validation is to compare GGM02S and the local solution for one month, namely August 2003, with GGM02C. Since the latter contains more gravitational signal and has less topographic correlation (cf. figure 1), it can be used as a reference. The comparison in figure 5 shows reduced and less regular variations for the local solution. The RMS reduces from 83.3 cm to 69.7 cm.

Next, the K-band range rate can again be compared to the relative velocity of the two satellites derived for the 6-min arc crossing the Himalayan mountain ridge. The fit can be quantified by differencing the crosscorrelation of GGM02C with the orbit arcs derived from GGM02S and from the local solution, respectively. Looking at the result in figure 6, the local model reduces the topographic correlation up to 50% peak to peak but is not able to remove it completely. We analysed all arcs crossing the area of interest in the year 2003 (cf. table 1) and the local solutions show consistently an improvement up to 40% with the exception of a few spurious arcs. Note that the instrument data at the beginning of the

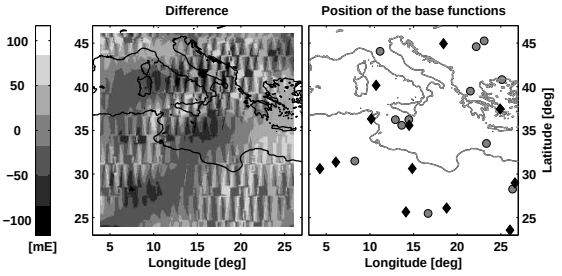

Figure 4. Closed-loop simulation: difference between input and approximation (left), position of the base function (right)

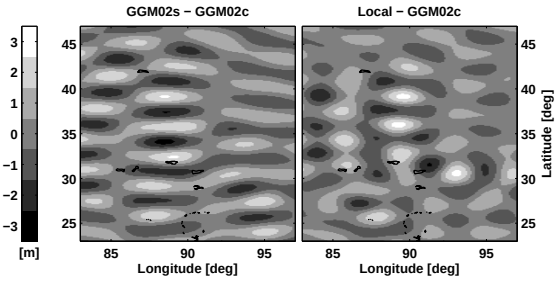

Figure 5. Geoid height differences w.r.t. GGM02C in August 2003: GGM02S (left) and local solution (right)

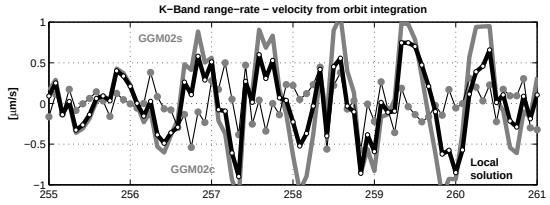

Figure 6. K-band observation versus velocity difference

Table 1. Statistics for arcs crossing the Himalayan area in 2003

Period	# arcs total	improvement +	-	Max	Mean
Jan. - Mar.	138	120	18	39%	11.1%
Apr. - Jun.	138	135	3	29%	15.0%
Jul. - Sep.	135	131	4	38%	13.7%
Oct. - Dec.	142	142	0	33%	12.9%

mission is of less quality than e.g. since March 2003 (pers. com. Frank Flechtner).

Since the results show a reduced correlation with the topography and the contribution of the possible error sources are only poorly correlated with the latter, we can conclude that the solution must contain additional gravitational information. The data processing is not optimized yet and a topographic correlation is still visible. Background models are still based on global data sets and the optimization process is based on empirical tests. It is expected that further improvements are possible and thus the results have to be considered preliminary.

4 Conclusions

In conclusion, a framework has been created in order to derive a refined model for the gravity field in local areas using the LOS gradiometry in combination with position optimized radial base functions. The approach promises to reveal further details in the level 1B data of the GRACE mission since the solutions can be tailored to local areas. The usage of the position optimized radial base functions avoids overparametrization and yields a stable system at the cost of a non-linear optimization problem. It has been shown with simulated and real data, that the approach can be successfully implemented. In further studies the trackiness and a refined background modeling need to be addressed.

Acknowledgments. We like to thank Dr. Frank Flechtner for his helpful review and his hint that till March 2003 the data is of less quality. Also the detailed suggestions of one anonymous reviewer helped to improve this paper and are highly appreciated.

References

Eicker, A., Gravity field refinement by radial base functions from in-situ satellite data, Ph.D. thesis, Rheinische Friedrich-Wilhelms-Universität zu Bonn, 2008.

Han, S., and F. Simons, Spatiospectral localization of global geopotential fields from the Gravity Recovery and Climate Experiment (GRACE) reveals the coseismic gravity change owing to the 2004 Sumatra-Andaman earthquake, *J. Geophy. Res.*, *113*, B01,405, doi:10.1029/2007JB004927, 2008.

Han, S., C. Jekeli, and C. Shum, Time-variable aliasing effects of ocean tides, atmosphere, and continental water mass on monthly mean GRACE gravity field, *J. Geophy. Res.*, *109*, B04,403, doi: 10.1029/2003JB002501, 2004.

Kanzow, T., F. Flechtner, C. A., R. Schmidt, P. Schwintzer, and S. U., Seasonal variation of ocean bottom pressure derived from Gravity Recovery and Climate Experiment GRACE: Local validation and global patterns, *J. Geophy. Res.*, *110*, C09,001, 2005.

Kaula, W., *Theory of satellite geodesy*, Blaisdell Publishing Company, 1966.

Keller, W., and M. Sharifi, Satellite gradiometry using a satellite pair, *J. Geod.*, *78*, 544–557, 2005.

Koop, R., Global gravity field modelling using satellite gravity gradiometry, Ph.D. thesis, Technische Universiteit Delft, Delft, Netherlands, 1993.

Marquardt, D., An algorithm for least-squares estimation of nonlinear parameters, *J. Appl. Math.*, *11*, 431–441, 1963.

Mayer-Gürr, T., Gravitationsfeldbestimmung aus der Analyse kurzer Bahnbögen am Beispiel der Satellitenmissionen CHAMP und GRACE, Ph.D. thesis, Rheinische Friedrich-Wilhelms-Universität zu Bonn, 2006.

Ortega, J., and W. Rheinboldt, *Iterative Solution of Nonlinear Equations in Several Variables*, Academic Press, NY, 1970.

Perosanz, F., R. Biancale, J. Lemoine, N. Vales, S. Loyer, and S. Bruinsma, Evaluation of the CHAMP Accelerometer on Two Years of Mission, in *Earth Observation with CHAMP*, edited by C. Reigber, H. Lühr, P. Schwintzer, and J. Wickert, pp. 77–82, Springer, 2005.

Rummel, R., C. Reigber, and K. Ilk, The use of satellite-to-satellite tracking for gravity parameter recovery, in *Proceedings of the European Workshop on Space Oceanography, Navigation and Geodynamics (SONG)*, 1978.

Schmidt, M., M. Fengler, T. Mayer-Gürr, A. Eicker, J. Kusche, L. Sánchez, and S. Han, Reginonal gravity modeling in terms of spherical base functions, *J. Geod.*, *81*, 17–38, doi: 10.1007/s00190-006-0101-5, 2007.

Schmidt, R., F. Flechtner, U. Meyer, C. Reigber, F. Barthelmes, C. Förste, R. Stubenvoll, R. König, K.-H. Neumayer, and S. Zhu, Static and Time-Variable Gravity from GRACE Mission Data, in *Observation of the Earth System from Space, ISBN 3-540-29520-8*, edited by J. Flury, R. Rummel, C. Reigber, M. Rothacher, G. Boedecker, and U. Schreiber, pp. 115–129, Springer, Berlin, 2006.

Tapley, B., J. Ries, S. Bettadpur, D. Chambers, M. Cheng, F. Condi, B. Gunter, Z. Kang, P. Nagel, R. Pastor, T. Pekker, S. Poole, and F. Wang, GGM02 - An improved Earth gravity field model from GRACE, *J. Geod.*, *79*, 467 – 478, doi: 10.1007/s00190-005-0480-z, 2005.

Wagner, C., D. McAdoo, J. Klokočník, and J. Kostelecký, Degradation of geopotential recovery from short repeat-cycle orbits: application to GRACE monthly fields, *J. Geod.*, *80*(2), 94–103, 2006.